PERGAMON

International Journal of Solids and Structures 40 (2003) 271–294

INTERNATIONAL JOURNAL OF SOLIDS and STRUCTURES

www.elsevier.com/locate/ijsolstr

Fracture of shape memory CuAlNi single crystals

G.M. Loughran [1], T.W. Shield *, P.H. Leo

Department of Aerospace Engineering and Mechanics, 107 Akerman Hall, 110 Union St. SE, University of Minnesota, Minneapolis, MN 55455, USA

Received 29 April 2002; received in revised form 4 September 2002

Abstract

The fracture behavior of shape memory CuAlNi single crystals loaded in tension is studied. Specimens cut from a single crystal are notched and loaded in tension until final fracture. Eight different crystallographic orientations of the notch and tensile axes are considered. The stress field at the notch tip triggers a cubic to orthorhombic phase transition in the crystal, which results in a set of twinned martensite plates emanating from the notch tip. As loading increases, a crack forms and grows off the notch tip, with the martensite plates continuing to appear at the growing crack. Details of the crack growth depend strongly on both the type of singular microstructures that forms and how this microstructure interacts with the growing crack. In one group of orientations a distinct transformation zone forms along one flank of the crack and the motion of this zone is directly connected to the crack growth. In a second group of orientations, the microstructure formation is not as strongly tied to the crack. Interestingly, in all specimens studied, the final crack direction is approximately 80° from the direction of the martensite plates.

Keywords: Fracture mechanics; Microstructure; Shape memory alloy; Single crystal

1. Introduction

Shape memory alloys (SMAs) such as CuAlNi, NiTi, CuZnAl and AuCuZn have received much attention in recent years owing to their applications in active structures, actuators and medical devices. SMAs undergo a diffusionless, structural, and reversible martensitic phase transformation. The martensitic transformation is accompanied by large shear-like deformation, which allows the material to deform up to 20 times a typical elastic deformation.

Copper-based SMAs are particularly interesting because of their low cost and relative ease of processing. However, copper alloys possess low strength (compared to NiTi alloys, for example) and also exhibit a degradation of shape memory capacity when thermally cycled. Many investigations have been made to improve the mechanical properties of polycrystalline Cu-based SMAs. Microalloying additions of Ti, Ni, Zr (Kim et al., 1990) as well as thermomechanical treatments have been used (Lai et al., 1996) to refine the

* Corresponding author. Tel.: +1-612-626-7793; fax: +1-612-626-1558.
E-mail address: shield@aem.umn.edu (T.W. Shield).
[1] G.M. Loughran was formerly G.M. Vasko.

0020-7683/02/$ - see front matter © 2002 Elsevier Science Ltd. All rights reserved.
PII: S0020-7683(02)00550-4

grain size, which results in an increase in fracture strength of up to 250% and an increase in elongation at fracture of up to 200%.

Among the Cu-based SMAs, CuAlNi and CuZnAl seem most attractive as replacements for expensive NiTi alloys, the material most often used for practical applications. The CuAlNi system is one of the more extensively studied systems owing to the ease of alloy preparation and the simplicity with which the critical transformation temperatures can be controlled by varying the nickel and aluminum content. However, the mechanical properties of these alloys are complicated by the fact that martensites can form with two different crystallographic structures: orthorhombic and monoclinic. Some investigations have been made to study the transition between stress-induced martensites in CuAlNi (Rodriguez and Brown, 1976; Sittner et al., 1998) as well as the behavior of the different martensites (Fang et al., 1999; Otsuka et al., 1974; Shield, 1995).

While there have been many studies of the thermomechanical properties of SMAs, there has been less work on their fracture. However, using austenite to martensite transformations to toughen a material is the basis for transformation-toughened ceramics (Simha and Truskinovsky, 1994). For example, Zirconia inclusions embedded in a ceramic may undergo a martensitic transformation near crack tips, which effectively toughens the ceramic. Also, Shimamoto et al. (1996) used shape memory NiTi fibers in an epoxy matrix to increase the fracture toughness of the composite. The resulting composite showed properties such as self-strengthening by compressive stresses in the matrix resulting from phase change of the embedded NiTi fibers.

In order to understand the factors controlling crack growth and material toughness in SMAs, it is necessary to consider material transformation at the crack tip. Dang and Grujicic (1997) have investigated crack tip transformation in FeNi austenite. They used atomistic simulations to show that martensitic transformation as well as crack tip material evolution involving dislocation emission leads to blunting of the crack tip and in turn to enhanced material toughness. Wang et al. (1991) has reported experiments in which this blunting effect was observed owing to martensitic transformation in the vicinity of microcracks in CuZnAl. Shek et al. (1997) have investigated the toughness of the austenite and martensite phases of CuAlNi single crystals by studying the fractal properties of the crack surface. Birman (1998) has looked at the relationship between phase transformations and the plastic zone at a crack tip during Mode I cracking of a Nitinol-55 (NiTi) plate.

In this research, the interaction between martensitic phase transformation and fracture is studied by conducting experiments on single crystal CuAlNi. Specimens cut from a single crystal are notched and loaded in tension. In previous work (Vasko et al., 2002), the martensitic microstructures that form at the notch were compared to those predicted by the Crystallographic Theory of Martensite (CTM) and selected according to an available work criterion. In this paper, the same specimens are loaded to final fracture, and the effect of the martensite on the fracture process is studied. As in Vasko et al. (2002), eight different crystallographic orientations of the notch and tensile axes are considered. The different orientations have different martensitic microstructures at the crack tip. As loading increases, a crack initiates and grows from the notch tip and the martensitic microstructure grows along with the crack. Details of the crack growth depend strongly on both the type of martensitic microstructures that forms and how this microstructure interacts with the growing crack.

In Section 2, the experimental procedures and specimen design are discussed. In Section 3, a brief summary of the available work criterion for selecting crack tip microstructures is given, based on Vasko et al. (2002). In Section 4, the experimental results on the fracture process in each specimen are presented. In Section 5, these results are discussed and analyzed and in Section 6, some conclusions are made.

2. Experimental procedure

As in Vasko et al. (2002), eight specimen orientations were chosen for the experimental study. The eight orientations are specified by a notch coordinate system x_n, y_n, z_n, where y_n is the tensile direction, z_n is

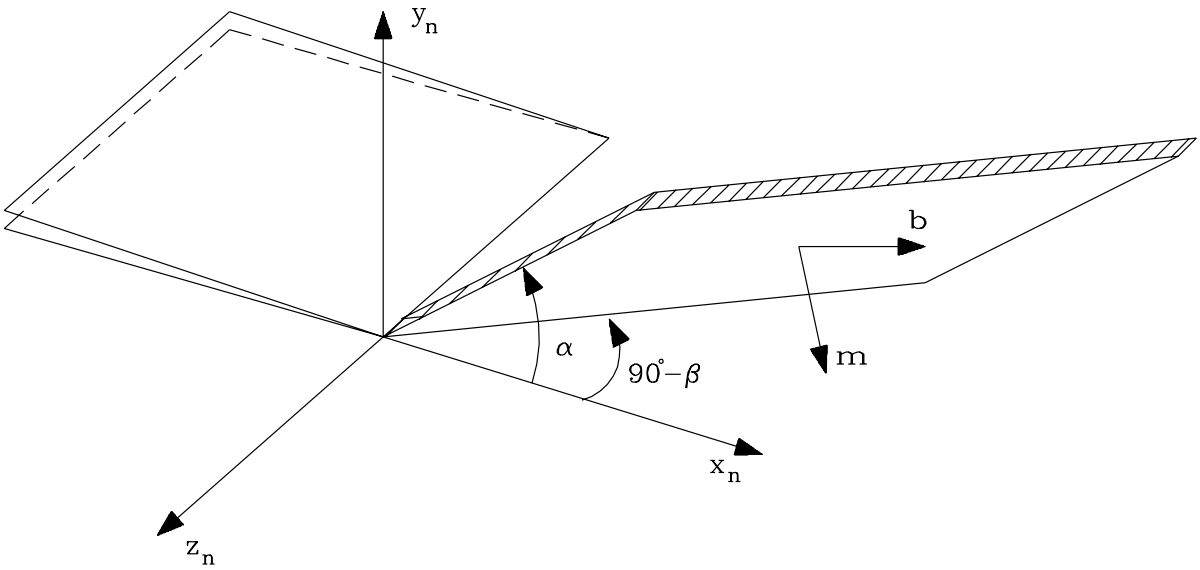

Fig. 1. The Cartesian coordinate system associated with the notch is shown with x_n taken as the notch direction, y_n as the notch plane normal and z_n as the surface normal, which is also the direction along the notch tip. The martensite plate at the notch is oriented at an angle α from the x_n-direction in the (x_n, y_n) plane (the in-plane angle) and at an angle $90° - \beta$ from the x_n-direction in the (x_n, z_n) plane (the out-of-plane angle).

normal to the specimen surface and along the notch tip and x_n is perpendicular to both y_n and z_n (see Fig. 1 and Table 1). All specimens have $z_n \| [1\bar{1}0]$; however, their x_n- and y_n-directions are different. Following Vasko et al. (2002), the eight orientations are labeled I–VIII.

The specimens were cut from a single crystal CuAlNi boule with composition of Cu-13.95 wt% Al-3.93 wt% Ni. The growth of the single crystal boule is reported in Vasko (2001). Different geometries were used to investigate fracture behavior, including a single edge notch (SEN) geometry, a modified single edge notch (MSEN) geometry and a compact tension (CT) geometry. Details of the specimen shapes are given in Fig. 2.

The heat treatment and specimen preparation process are identical to those reported in Vasko et al. (2002). After being cut from the boule each SEN and MSEN specimen was cut in half along the thickness direction to give a pair of specimens (a and b in Table 1). Each specimen was then heat treated at 990 °C for

Table 1
Orientations and geometry of the specimens used in this study

Orientation	Notch normal y_n	Notch tip z_n	Specimens	Geometry
I	$[001]$	$[1\bar{1}0]$	T4a*, T4b	SEN, SEN
II	$[\overline{0.70}, \overline{0.70}, \overline{0.14}]$	$[1\bar{1}0]$	T5b*, T6a, T6b, T8a, CT2	SEN, SEN, SEN, MSEN, CT
III	$[\overline{0.61}, \overline{0.61}, \overline{0.50}]$	$[1\bar{1}0]$	T7a, T7b*, T9a*, CT1	SEN, SEN, MSEN, CT
VI	$[\overline{0.61}, \overline{0.61}, 0.50]$	$[1\bar{1}0]$	CT3	CT
V	$[\overline{0.07}, \overline{0.07}, 0.99]$	$[1\bar{1}0]$	CT4*	CT
VI	$[\overline{0.07}, \overline{0.07}, \overline{0.99}]$	$[1\bar{1}0]$	CT5	CT
VII	$[0.24, 0.24, \overline{0.94}]$	$[1\bar{1}0]$	CT6*	CT
VIII	$[\overline{0.37}, \overline{0.37}, 0.85]$	$[1\bar{1}0]$	CT7*	CT

The specimen geometries are SEN, MSEN and CT as shown in Fig. 2. The notch tip direction is also the normal to the plane of observation. Specimens marked with an asterisk are the ones that appear in the images.

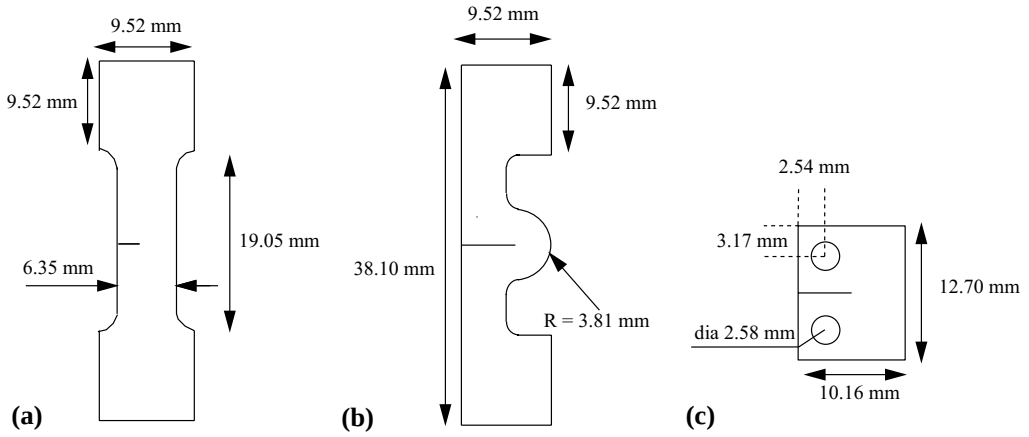

Fig. 2. The shapes of the specimens used in this study are shown: (a) SEN specimens have a 2.54 mm notch length and a nominal thickness of 1.27 mm, (b) MSEN specimens have a 5.71 mm notch length and a 1.27 mm nominal thickness and (c) CT specimens have a 5.08 mm long notch and a 2.54 mm nominal thickness.

one hour and quenched in ice water (≈0°C). During heat treatment specimens with orientations II and III were clamped between graphite blocks to reduce warping. One or both surfaces of the specimens were mechanically polished on a heated stage at 65 °C. Finally, a 50 μm diameter wire in an Electrical Discharge Machine with a specimen holder heated to above 80 °C was used to cut the notch. The notches are 2.5 mm long and 100 μm wide.

Uniaxial tension experiments were performed on each notched specimen using an Instron 4502 load frame. The SEN and MSEN specimens were held by microwedge grips. The CT specimens were loaded by clevises that are held by these wedge grips. The crosshead speed was 0.01 mm/min for all experiments. All specimens were heated by circulating water through coils of copper tubing that surround the grips. The Instron was controlled in displacement with a 586 class microcomputer. Microstructures on the polished specimen surface(s) were observed using a high resolution JVC single-chip color CCD camera attached to a metallurgical microscope. The video signal from the video camera was recorded using a SVHS video tape recorder. Color images were also digitized using an SGI O2 workstation equipped with an MVP video board.

Once a specimen was installed in the grips, it was heated to 80 °C to make sure it was completely austenitic. The experiment on the specimen was performed at 50 °C nominal water bath temperature. The specimen temperature was 3–5° cooler. Any specimen that underwent load/unload cycling was reheated to 80 °C after each unloading.

A total of 16 specimens were designed for the fracture study. Two specimens (T4a and T4b) have orientation I, five specimens (T5b, T6a, T6b, T8a and CT2) have orientation II, four specimens (T7a, T7b, T9a and CT1) have orientation III, and there is one specimen with each of the orientations: IV(CT3), V(CT4), VI(CT5), VII(CT6) and VIII(CT7).

The eight orientations (defined by their (x_n, y_n, z_n) notch coordinate systems), shown schematically in Fig. 3, are divided into two groups, based on their orientations and on similarities in their fracture behavior. Group 1 (Fig. 3) includes orientations with x_n-directions centered about the crystallographic [0 0 1] axis. These orientations are II, III and IV, with the x_n-directions at 8°, 30° and −30° respectively from the [0 0 1] cubic axis.

Group 2 includes orientations I, V, VI, VII and VIII, with x_n-directions centered about the crystallographic [1 1 0] axis (see Fig. 3). The x_n-directions for these orientations are 0° (I), 6° (V), −6° (VI), 20° (VII) and 32° (VIII) from the [1 1 0] cubic axis.

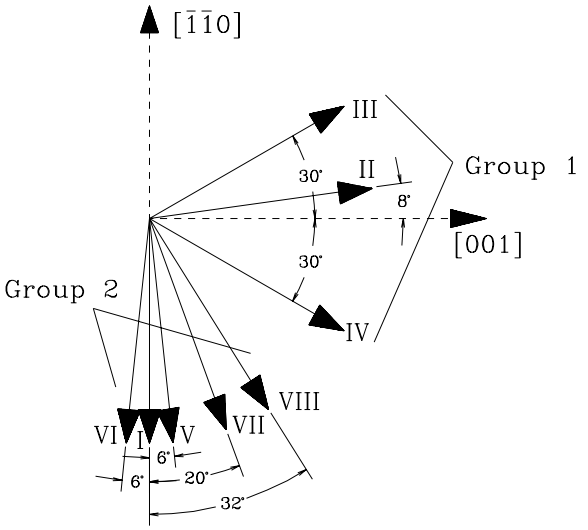

Fig. 3. The eight orientations I–VIII are shown relative to the [0 0 1] and [1̄ 1̄ 0] directions in the plane of the specimen. The arrows indicate the x_n-direction for each orientation. The orientations are divided into two groups. Group 1 includes orientations with the x_n-direction centered about the [0 0 1] cubic axis and Group 2 includes orientations with the x_n-direction centered about the [1 1 0] cubic axis.

3. Notch tip microstructures

The selection of notch tip microstructures has been discussed extensively in previous work (Vasko et al., 2002). Here, the selection criterion is briefly presented in order to introduce necessary notation and nomenclature.

It was shown in Vasko et al. (2002) that the microstructures that form at the notch tip are consistent with CTM predictions of austenite–martensite (AM) interfaces separating an austenite phase from a twinned martensite plate. For the CuAlNi system, which undergoes a cubic to orthorhombic transition, there are 96 possible AM interfaces. These interfaces are characterized by the normal **m** to the interface and the shear vector **b** of the interface. The projection of the normal **m** onto the x_n–y_n plane of each specimen defines the in-plane angle α of that AM interface (see Fig. 1 and Table 2). Details of the AM interfaces, including the labels used in Table 2, are given in Vasko et al. (2002).

Of all possible AM interfaces (also referred to as microstructures), those that appear at the notch tip can be predicted based on the work available from the stress field to transform to each AM interface. Consider a stress field from a plane problem that has components $\sigma_{ij}(r,\theta)$ in a rectangular Cartesian coordinate system $(x_1,x_2,x_3)=(x_n,y_n,z_n)$, where r and θ are polar coordinates centered on the notch tip in the x_n–y_n plane. [2] Then the work available to transform to AM interface k ($k=1,\ldots,96$) with normal $\mathbf{n}^{(k)}$ (components $n_i^{(k)}$) and shear vector $\mathbf{b}^{(k)}$ (components $b_i^{(k)}$) is

$$W^{(k)}(r,\theta)=\sigma_{ij}(r,\theta)n_j^{(k)}b_i^{(k)}, \tag{1}$$

where repeated indices imply summation over 1, 2, 3 and indices in parenthesis are not summed. Because this criterion is intended as a relative criterion among the 96 AM interfaces, the applied stress intensity factor may be scaled out. In addition, because all the components of the stress field have the same variation

[2] In Vasko et al. (2002), this field is given by the asymptotic elastic crack tip stress field solution of Sih et al. (1965).

Table 2
Predicted AM interfaces near a crack tip in orientations I–VIII and the observed interface angles

Orientation	Predicted AM interfaces				Observed interfaces	
	First		Second		First	Second
	Label	α_1	Label	α_2	α_1	α_2
I	$\mathscr{E}/\mathscr{F}$	±27.5°			27°	−27°
II	$\mathscr{A}$	−55.2°	$\mathscr{A}$	−55.2°	−55°	(39°)
III	$\mathscr{A}$	−77.2°	$\mathscr{C}$	86.9°	−77°	87°
IV	$\mathscr{B}$	77.2°	$\mathscr{D}$	−86.9°	77°	−87°
V	$\mathscr{F}$	−33.5°	$\mathscr{E}$	21.5°	−33°	20°
VI	$\mathscr{E}$	33.5°	$\mathscr{F}$	−21.5°	33°	−20°
VII	$\mathscr{F}$	−47.5°	$\mathscr{E}$	7.5°	−47°	5°
VIII	$\mathscr{F}$	−59.5°	$\mathscr{F}$	−59.5°	−59°	–

The angles α_1 and α_2 are the in-plane angles of the predicted and observed AM interfaces. The quantities marked first are predicted/observed to occur before the second quantities. The value of α_2 in parentheses indicates that only a very small amount of this interface was observed on one side of the specimen. See Vasko et al. (2002) for the identification of the microstructures from the labels.

with r, the r-dependence may be ignored. At each θ, the specific AM microstructure (value of k) that maximizes $W^{(k)}$ is selected; this gives the available work $W(\theta)$. In most cases a plot of $W(\theta)$ against θ reveals that there is a global maximum at some θ associated with the primary microstructure, and a local maximum at a different θ (far from the first) associated with the secondary microstructure. These microstructures were found in all cases to have in-plane angles that agreed with the experimental results, and are the microstructures seen in the fracture studies presented below. In addition, a larger amount of the primary microstructure appears compared to the secondary microstructure. A comparison of the predictions of the available work criteria with the experimental observations is summarized in Table 2.

4. Fracture

After the appearance of the initial microstructures at the notch tip as described in Vasko et al. (2002), loading was continued until crack growth occurred. In many cases the specimen was unloaded, heated, cooled and then reloaded before the crack was allowed to run to the specimen edge. Detailed results for this process are now given. It should be noted that, with one significant exception, the results for a given orientation were consistent for all specimens and specimen geometries. Hence only selected results from each orientation are discussed. The results are organized into two groups based on orientation and fracture behavior.

4.1. Group 1

Group 1 includes orientations with the x_n-directions centered about the crystallographic [0 0 1] axis. These orientations are II, III and IV, with x_n-directions at 8°, 30° and −30° from [0 0 1]. A summary of the specimen orientations is given in Table 1 and Fig. 3.

4.1.1. Orientation II

Orientation II has its x_n-direction at 8° from the [0 0 1] cubic axis (Fig. 3). Five specimens with orientation II were tested. Four were heat treated so as to exhibit the martensitic phase transformation, while one was not heat treated and so did not phase transform. The non-transforming specimen fractured in a brittle manner and in a completely different direction from the heat treated specimens. All specimens that showed

a phase transformation behaved similarly, and so the data presented is from one of the specimens, labeled T5b.

Specimen T5b underwent three loading cycles. Between each loading cycle the specimen was heated to 80 °C to remove all martensite. The load–displacement curves for the first two loading cycles are shown in Fig. 7. The points on the curves correspond to conditions for the images in the figures discussed below. Experimental data from the first loading of the specimen is presented in Fig. 4. The sequence of images (a)–(e) shows formation of the microstructure prior to the fracture as load increases. A martensitic microstructure with in-plane angle of −55° relative to the x_n-direction is induced at the notch tip (Fig. 4(a)). As seen in

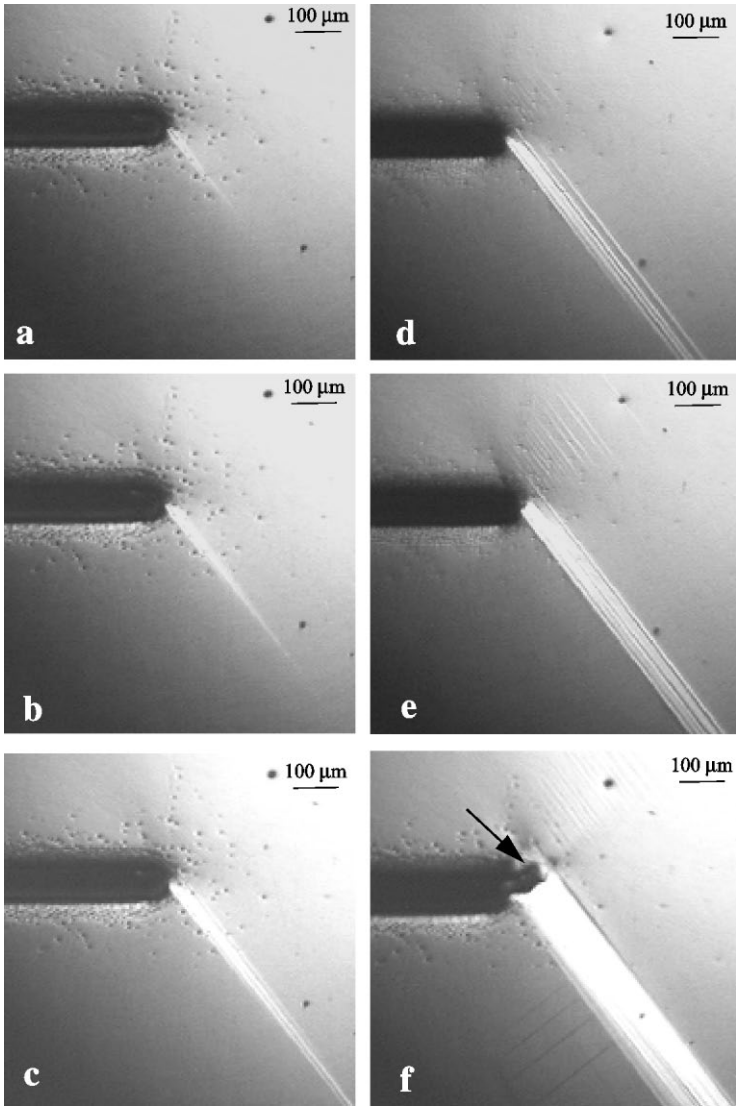

Fig. 4. A sequence of images showing the formation of a transformation zone during the first loading of specimen T5b with orientation II is presented. The light lines are the martensite bands, which form at −55° relative to the x_n-direction. These images were taken at the following points on the load–displacement curve Fig. 7(a) at: (a) 2, (b) 3, (c) 4, (d) 5, (e) 7 and (f) 8.

Figs. 4(b)–(e), the formation of new bands of this microstructure occurs in a well-defined region or transformation zone along the notch flank.

The formation of the transformation zone is followed by the initiation of the crack, marked by an arrow in Fig. 4(f). After the initiation of the crack the specimen was unloaded. During unloading most of the material transforms back to austenite, and only a short martensite band is left at the tip of the new crack. This band disappears on heating and a small amount of martensite reappears at the crack tip on cooling.

Figs. 5 and 6 show data taken during the second loading of the specimen. Figs. 5(a) and (b) show the −55° microstructure that develops along the crack. As in the initial loading, the martensite forms in a well-

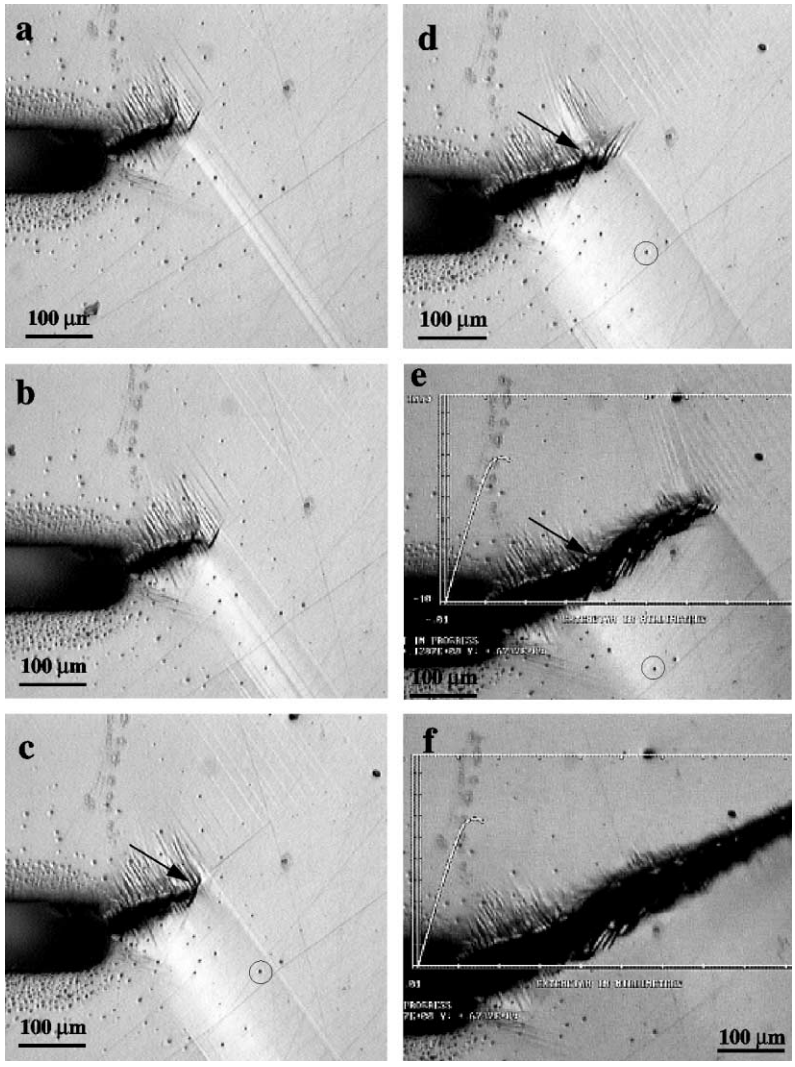

Fig. 5. The fracture process in specimen T5b with orientation II during the second loading is shown. The sequence of images shows formation of the −55° microstructure at the crack tip (a, b), the stable crack growth (c–e) and unstable crack extension (f). (The image (e) was taken just before unstable crack growth occurred.) Arrows in (c–e) mark a reference point on the crack edge to show the stable crack propagation. A point on the specimen surface is marked by circles in (c–e) to highlight the change in the transformation zone during stable crack growth. These images were taken at the following points on the load–displacement curve Fig. 7(b) at: (a) 1, (b) 2, (c) 3, (d) 4, (e) 5 and (f) 6.

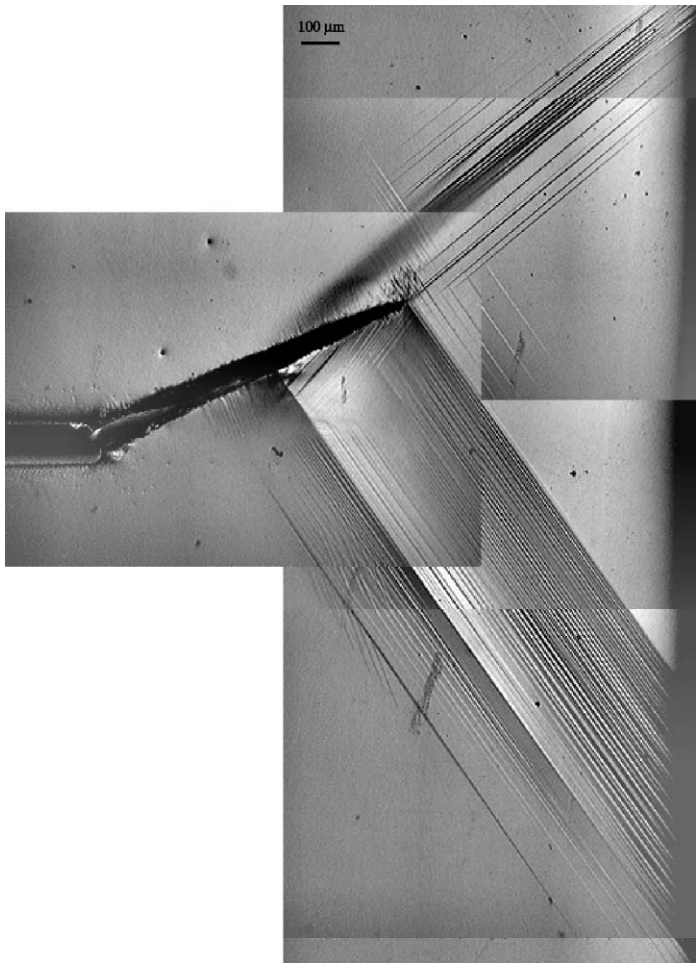

Fig. 6. A large view of specimen T5b with orientation II is presented after two periods of unstable crack growth. Note that material transforms back to austenite in the wake of the stable crack growth (see Fig. 5). The −55° microstructure forms a transformation zone at the tip of the arrested crack. New microstructure with an in-plane angle of 39° appears above the crack tip. This image was taken at the point on the load–displacement curve Fig. 7(b) labeled 10.

defined transformation zone, as shown in Fig. 5(c). Upon further loading, the crack grows in a stable manner. Here, stability is characterized by the fact that the crack grows only as the extension is increased and without a drop in load (see Fig. 7(b)). Because stable crack growth is tied to the extension rate, it is easy to follow. The arrows in Figs. 5(c)–(e) mark a reference point on the crack edge to show the crack extension. Stable crack extension is accompanied by the formation of new microstructure; the leading edge of the zone (at the crack tip) moves with the crack tip while the trailing edge (along the crack flank) is stationary. This is shown in Figs. 5(c)–(e), where circles mark a reference point on the specimen surface.

Stable crack growth is followed by an unstable growth burst, resulting in the large amount of crack growth between Figs. 5(e) and (f). These two images were taken at points 5 and 6 on the load–displacement curve shown in Fig. 7(b), which are at nearly the same extension. Unstable crack growth is characterized by the load drop seen between these points and occurs at a much faster rate than the imposed extension rate would dictate. After unstable growth arrested, it was observed that both the leading and trailing edges of

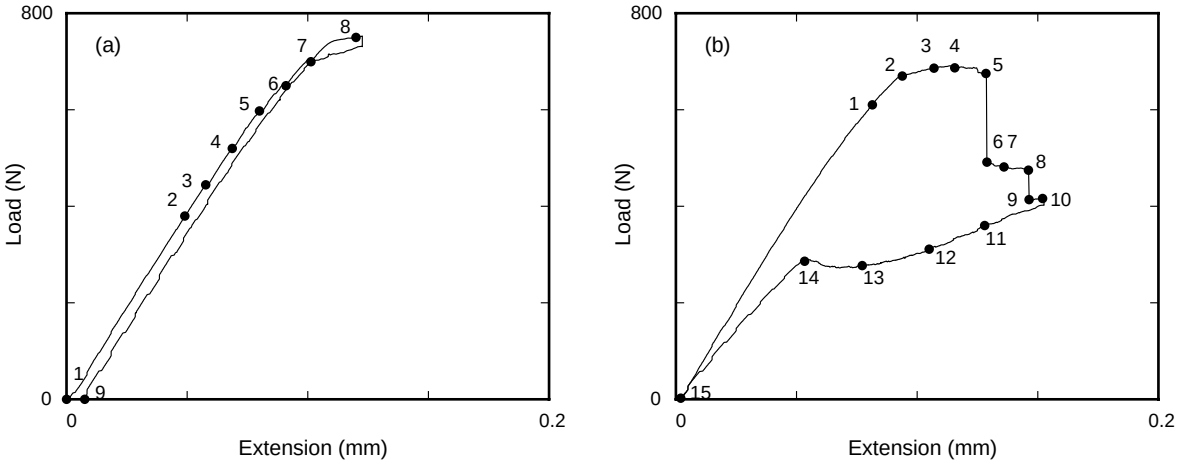

Fig. 7. The load–displacement curves for specimen T5b with orientation II are shown. Figure (a) shows the first loading cycle; (b) shows the second loading cycle. The circles represent the load level associated with the images presented in this work.

the transformation zone had moved with the crack tip. (The transformed material is no longer visible in Fig. 5(f).) The width of the transformation zone is relatively constant during this period as the material at the trailing edge of the zone transforms back to austenite. This process is clearer in the original video from which these static images were taken. High speed photography would give a better picture of the situation.

As the second loading cycle continues, a period of stable crack growth (points 6–8) is again followed by unstable growth (points 8 and 9) as can be seen in the load–displacement curve in Fig. 7(b). The transformation zone behavior during both stable and unstable crack growth follows the pattern described above. Fig. 6 shows the crack and microstructure at point 10 on Fig. 7(b). Note that the transformation zone has translated with the crack tip from its position in Fig. 5, indicating that some material has reverse transformed. Also, a secondary microstructure, with an in-plane angle of 39°, appears above the crack tip. On unloading, the trailing edge of the transformation zone begins reverse transformation immediately. After unloading the displacement is almost completely recovered, as shown by Fig. 7(b), and the crack is completely closed. This indicates that very little, if any, plastic deformation has occurred.

A third loading cycle was performed on specimen T5b. The pattern of microstructure formation during stable crack growth followed by a period of unstable crack growth was repeated as described above. The crack continued to propagate in the same direction until it reached the edge of the specimen. In fact the crack stayed straight throughout the three load cycles and made an angle of 22° relative to the notch x_n-direction.

4.1.2. Orientations III and IV

Orientation III has its x_n-direction at 30° from the [0 0 1] cubic axis, while orientation IV has its x_n-direction at −30° from the [0 0 1] cubic axis. The two symmetric orientations behaved identically and so only orientation III will be discussed. Note that the x_n-direction for orientation III is the same as the crystallographic fracture direction observed in orientation II. Also, the primary martensitic microstructure predicted and observed for orientation III has an in-plane angle of −77° from the x_n-direction. Because of the steepness of this microstructure and the aspect ratio of the SEN specimen, this microstructure does not intersect the free edge of the specimen but instead interacts with the grip region of the specimen. The MSEN

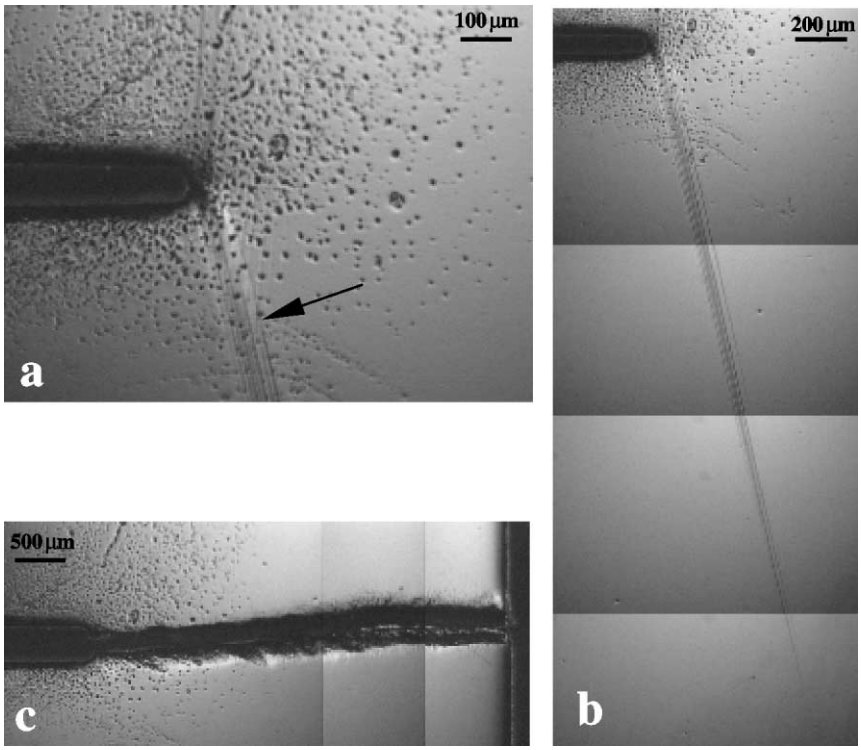

Fig. 8. The fracture process in specimen T7b with orientation III is shown. Microstructure with an in-plane angle of −77° forms at the notch tip prior to fracture, as indicated by an arrow in image (a). As seen in image (b), this microstructure has a large in-plane angle and grows toward the lower grip (grip is not shown). Image (c) shows the result of unstable fracture along the x_n-direction. These images were taken at the following points on the load–displacement curve Fig. 9 at: (a) 3, (b) 2 and (c) 5.

geometry was designed to alleviate this interaction. [3] Representative tests using both SEN and MSEN geometries are reported below.

The SEN specimen with orientation III is labeled T7b. In this specimen, microstructure at −77° was induced at the notch tip upon loading, as shown by an arrow in Fig. 8(a). As seen in Fig. 8(b), the microstructure grows toward the grips in the SEN specimens rather than towards the edge of the specimen. At the final point in the loading curve in Fig. 9 the crack propagation becomes unstable and the specimen fractures. No stable crack growth is observed. The crack propagates along the notch x_n-direction, as seen in Fig. 8(c).

The MSEN specimen with orientation III is labeled T9a. As with specimen T7b, the −77° microstructure initiates at the notch, as seen in Figs. 10(a) and (b). However, the microstructure now grows towards a free edge, which it reaches before a crack initiates. At this point, there is a significant increase in the amount of microstructure observed, especially as compared to specimen T7b. As observed for orientation II, the martensite forms in a well-defined transformation zone. Moreover, as loading continues, stable crack propagation is observed, and the transformation zone grows with the crack (see Fig. 10(b)). Stable crack propagation is followed by a period of unstable crack growth. This behavior can be observed in the loading curve for this specimen in Fig. 11.

[3] The CT geometry behaves similar to the MSEN geometry.

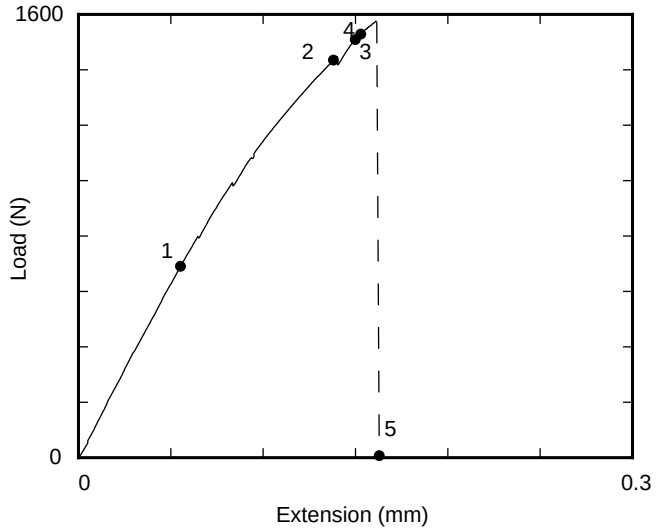

Fig. 9. The load–displacement curve for specimen T7b with orientation III is shown. The circles represent the load level associated with the images presented in this work.

During the experiment, a secondary microstructure, seen above the crack in Fig. 10(a) and (b), forms at 87° to the x_n-direction; however this microstructure does not show any correlation with the growing crack. The crack propagates straight across the material, as shown in Fig. 10(c), consistent with specimen T7b.

4.2. Group 2

Group 2 (Fig. 3) includes orientations with x_n-directions centered about the crystallographic [1 1 0] axis. These orientations are I, V, VI, VII and VIII, with x_n-directions at 0° (I), 6° (V), −6° (VI), 20° (VII) and 32° (VIII), respectively, from the [1 1 0] cubic axis. A summary of the specimens and their orientations is in Table 1.

4.2.1. Orientation I

Orientation I is highly symmetric and has its x_n-direction along the [1 1 0] axis. Two specimens with orientation I were tested, with similar results. The results below are from the specimen labeled T4a. Upon loading of this specimen, two microstructures were initiated at the notch tip, with in-plane angles of ±27° (see Fig. 12(a)). Another pair of microstructures with in-plane angles of ±40° developed as the load increased. However, the initial microstructures are more prevalent than the second microstructures.

Fig. 12 shows the fracture process at the crack tip. After the crack initiates, it grows in a stable manner at approximately 30° from the x_n-direction, as seen in Figs. 12(b) and (c). Note that the microstructures seem to overlap each other around the new crack, and do not form a well-defined transformation zone. As will be seen, this is a characteristic of Group 2 orientations. Upon continued loading the crack changes direction and propagates in an unstable manner for a short burst, as shown in Fig. 12(d), and indicated by the load drop in Fig. 13. The crack then resumes stable growth, albeit now at approximately −30° from the x_n-direction, as shown in Fig. 12(e). The crack eventually grows rapidly to final fracture, as shown in Fig. 12(f). The final crack growth direction is in the x_n-direction, though it is clear that the crack path is more complicated than in any other specimens.

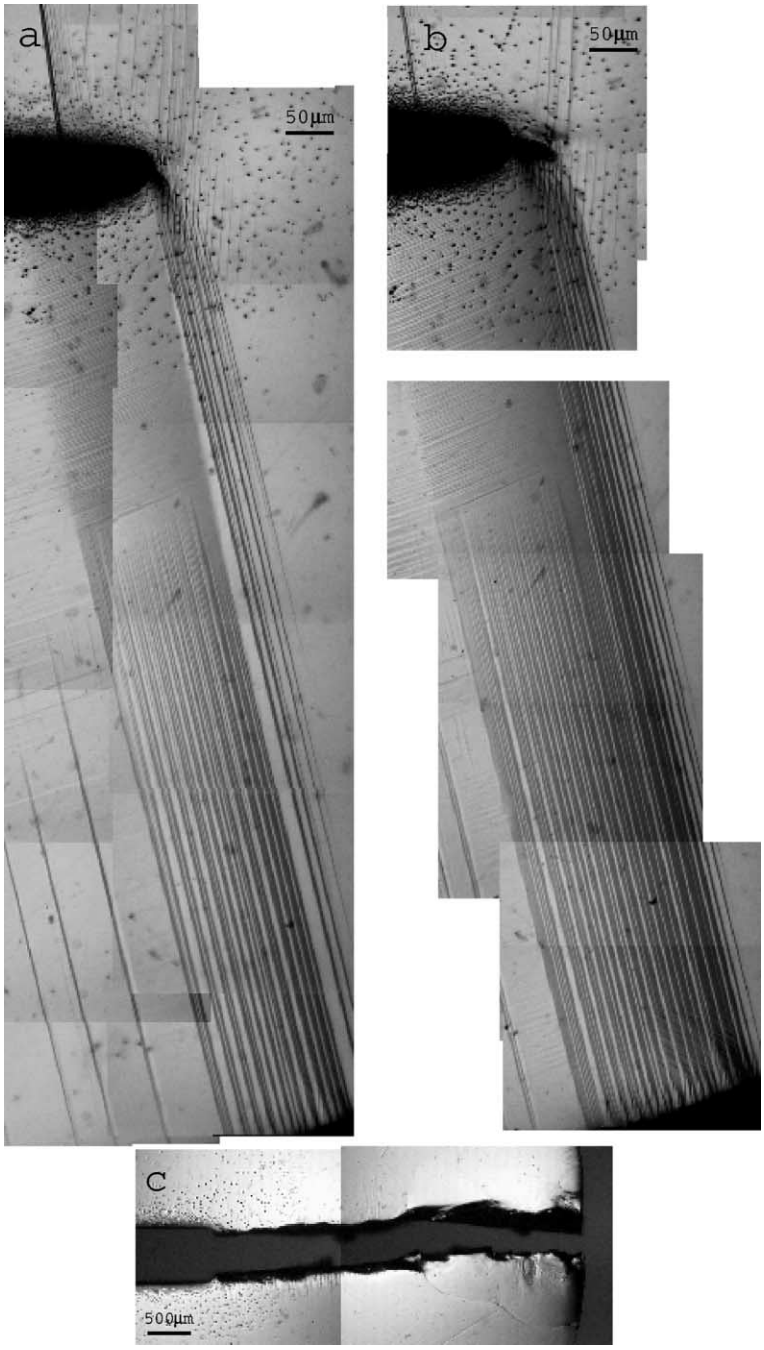

Fig. 10. The crack tip microstructure during the fracture process in specimen T9a with orientation III is shown. The shape of this MSEN specimen allows the −77° microstructure to reach a free edge (compare to the results from the SEN specimen T7b shown in Fig. 8(b)). The microstructure forms a transformation zone, which extends with the growing crack. Image (c) shows unstable crack extension along the x_n-direction. These images were taken at the following points on the load–displacement curve Fig. 11 at: (a) 2, (b) 3 and (c) 4.

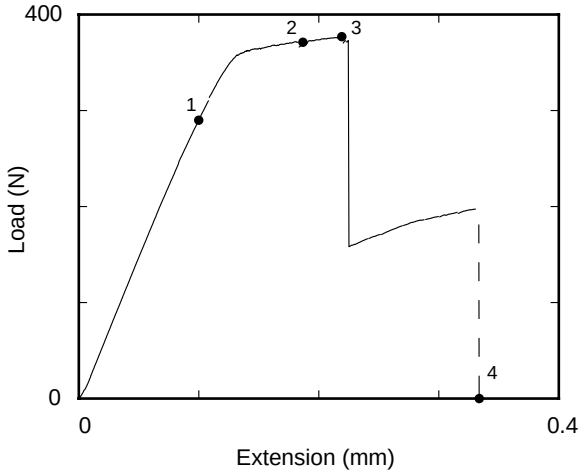

Fig. 11. The load–displacement curve for specimen T9a with orientation III is shown. The circles represent the load level associated with the images presented in this work.

4.2.2. Orientations V and VI

Orientation V has its x_n-direction at 6° from the [1 1 0] cubic direction. Orientation VI has its x_n-direction at −6° from the [1 1 0] cubic direction, and so it is symmetric to orientation V. Note that both specimens are at 6° from orientation I. One compact tension specimen with orientation V (CT4) and one with orientation VI (CT5) were tested. The results from the two tests are similar and so only results from orientation V are discussed.

The fracture process in orientation V is shown in Fig. 14. Because the high symmetry of orientation I is broken, the stress-induced microstructures are not symmetric, though they are the same ones that appear in orientation I. The first microstructure induced at the crack tip has an in-plane angle of −33°, while the second has in-plane angle 20°. The −33° microstructure appears to be present in a slightly greater amount than the 20° microstructure. The arrows in Fig. 14(d) mark both the −33° microstructure (arrows '1' and '3') and the 20° microstructure (arrows '2', '4'). Microstructures labeled '1' and '2' form in front of the notch tip, while those labeled '3' and '4' form mainly above and below the notch.

Fracture starts by initiation of two wing cracks from the notch, which are marked by arrows in Fig. 14(a). (The dark line in front of the notch is a scratch on the polished surface of the specimen.) As loading continues, these cracks grow, with the upper crack becoming longer than the lower one, as seen in Fig. 14(b). There is some microstructure formation at the tips of the wing cracks, with the −33° microstructure forming at the upper crack and the 20° microstructure forming at the lower crack. However, the microstructures at the wing cracks are only a small fraction of the total microstructure (see Fig. 14(d)).

Just after the image in Fig. 14(c) was taken, unstable crack propagation occurred from the upper wing crack, resulting in the crack shown in Fig. 14(e) and the large load drop in the load–displacement curve in Fig. 15. The direction of the final crack is approximately 43° from the x_n-direction. (Fracture in orientation VI is approximately −43° from its x_n-direction.) As seen in Fig. 14(e), this direction is different from the directions of the wing cracks.

4.2.3. Orientation VII

Orientation VII has its x_n-direction at 20° from the [1 1 0] cubic axis. One specimen (CT6) with orientation VII was fractured. The experimental data from this specimen is presented in Fig. 16. The first

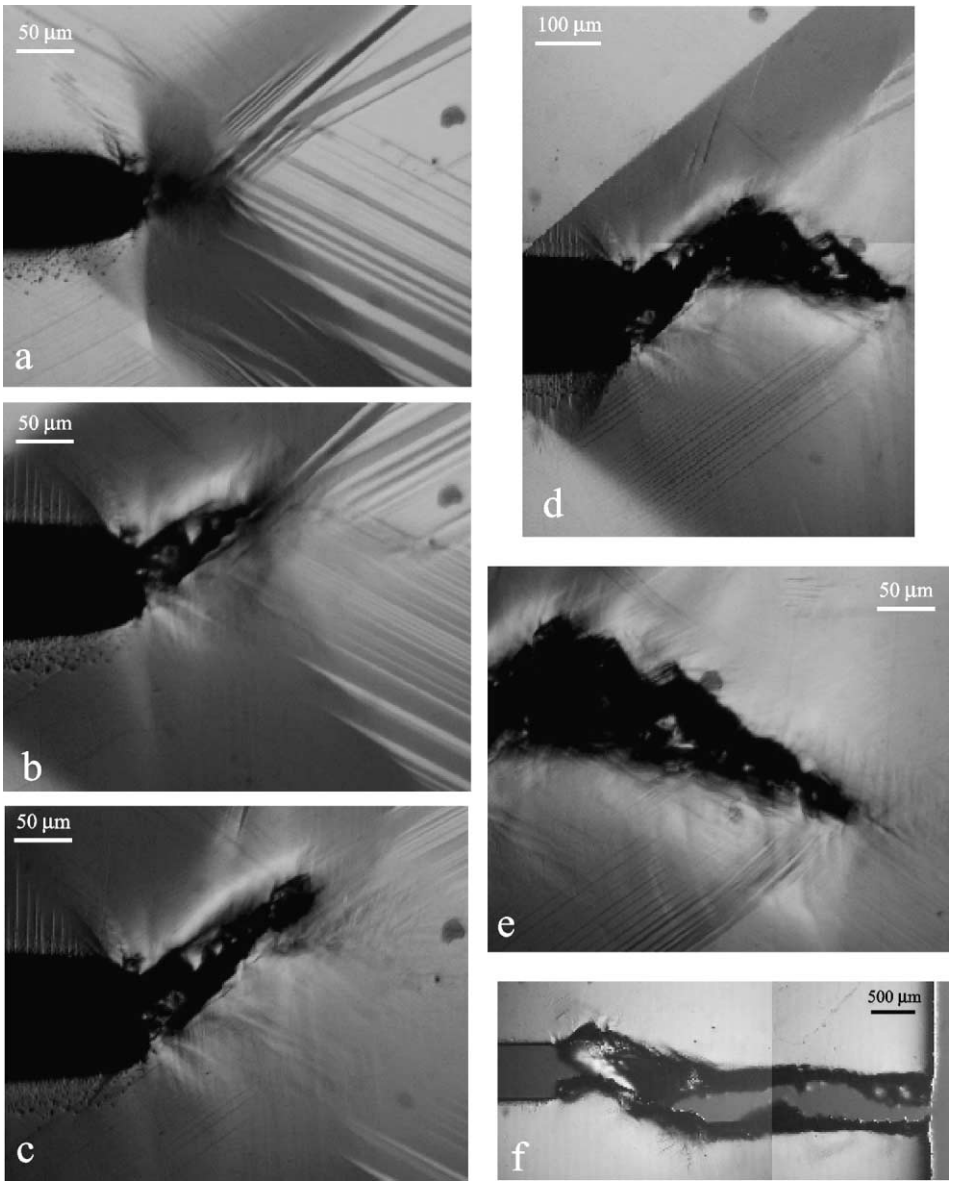

Fig. 12. The fracture process in specimen T4a with orientation I is shown. Image (a) shows the crack initiation; (b, c) shows stable crack growth at 30° relative to the x_n-direction; (d) shows the crack after unstable growth in a new direction of −30° relative to the x_n-direction; (e) shows further stable crack growth; (f) shows final fracture after unstable crack extension. These images were taken at the following points on the load–displacement curve Fig. 13 at: (a) 3, (b) 4, (c) 5, (d) 6, (e) 7 and (f) 8.

microstructure that appears at the notch tip has an in-plane angle of −47°, while the second has an in-plane angle of 4.5°. In Fig. 16(a), the −47° microstructure is marked by arrows '1' and '3' and the 4.5° microstructure is marked by arrows '2' and '4'.

Crack growth occurs initially by the formation of two wing cracks, marked by arrows in Fig. 16(b). These cracks grow in a stable manner, with the upper crack growing faster than the lower one. The −47°

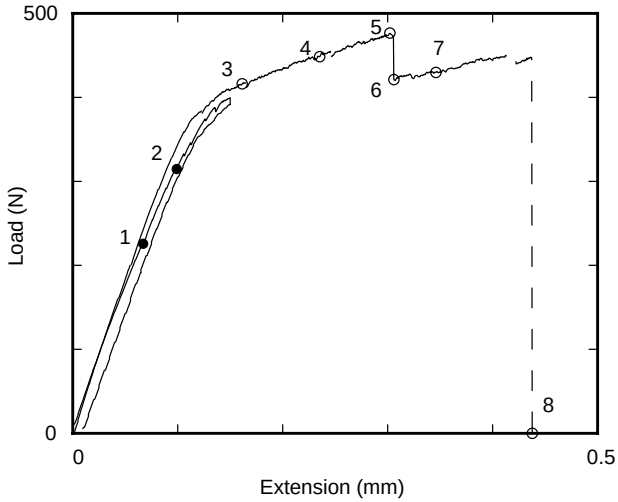

Fig. 13. The load–displacement curves for specimen T4a with orientation I are shown. The curve with solid circles is from the first loading cycle, and the curve with open circles is from the second cycle. The circles represent the load level associated with the images presented in this work.

microstructure is observed near the upper wing crack and the 4.5° microstructure is observed near the lower wing crack.

Fig. 16(d) shows the specimen just after unstable crack growth, which was accompanied by the large load drop in Fig. 17. This crack formed off the upper wing crack. The fracture direction is at 33° from the initial notch direction.

4.2.4. Orientation VIII

Orientation VIII has its x_n-direction at 32° from the [1 1 0] cubic direction. Note from Fig. 3 that orientation VIII is closer to the Group 1 orientations than are the other Group 2 orientations. One specimen (CT7) with orientation VIII was tested.

Experimental results from this specimen are shown in Fig. 18. Microstructures with in-plane angles −57° (arrow '1') and −3° (arrow '2') are observed around the notch tip during the fracture process. Stable crack propagation occurs as load increases, as shown in Fig. 18(b). During stable crack extension the amount of the −57° microstructure increases. Also the −3° microstructure forms below the notch after the crack begins to grow. Unstable crack growth occurs in a direction at approximately 26° from the x_n-direction (Fig. 18(c)) and is accompanied by a large load drop, Fig. 19. Note that the crack shown in Fig. 18(c) is almost entirely through the specimen and that the load at point 6 in Fig. 19 is not quite zero.

5. Discussion

This paper presents an initial investigation of the interaction between fracture and phase transformation in a CuAlNi SMA. Fracture and transformation behavior are found to be a function of the crystallographic orientation of the initial notch, and to a lesser extent, the specimen shape. The experimental results are summarized in Table 3. These results indicate that the initial orientation of the notch is the main variable affecting the fracture behavior. Specimen shape had a effect on the fracture process only for orientations III and IV.

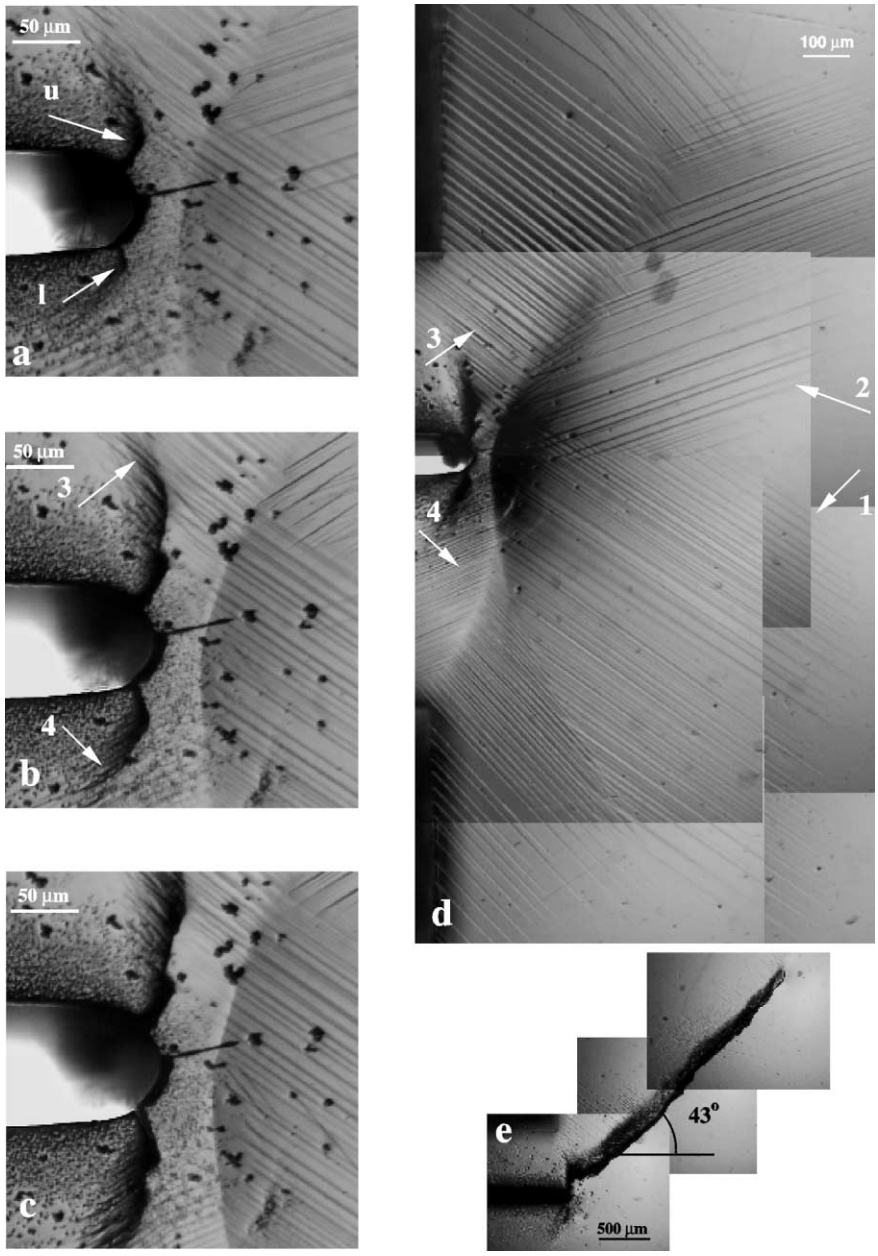

Fig. 14. The fracture process in specimen CT4 with orientation V is shown. The sequence of images (a–c) shows the growth of two wing cracks, marked by arrows in (a), accompanied by formation of the microstructure at their tip, marked by arrows in (b). Image (d) shows a larger view at the same load level as (b). The arrows in (d) indicate microstructures with in-plane angle of −33° ('1' and '3') and 20° ('2' and '4'). Growth of the wing crack is followed by unstable crack growth from the upper wing crack. A view of the final crack after unloading is shown in (e). These images were taken at the following points on the load–displacement curve Fig. 15 at: (a) 3, (b, d) 4, (c) 5 and (e) 6.

The eight specimen orientations chosen all have the $(1\bar{1}0)$ plane of the cubic austenite phase as the observation surface. The orientations were divided into two groups based on their x_n-direction (Fig. 3).

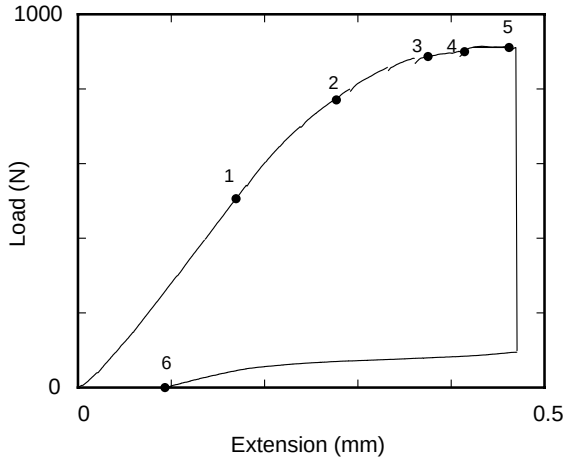

Fig. 15. The load–displacement curve for specimen CT4 with orientation V is shown. The circles represent the load level associated with the images presented in this work.

Orientations in Group 1 (II, III and IV) have their x_n-direction close to the [0 0 1] cubic direction, while orientations in Group 2 (I, V–VIII) have their x_n-direction close to the [1 1 0] cubic direction. The experimental data show that orientations in the same group behave similarly, while there are distinct differences between the behavior of orientations in different groups. The observed crystallographic fracture planes are also consistent within each group, but are different from group to group. Interestingly, the in-plane angle between the fracture direction and the primary AM microstructure was similar for all orientations in both groups.

The fracture processes in Groups 1 and 2 can be summarized as follows. Group 1 orientations all have a single microstructure that forms in a well-defined transformation zone along the notch flank. A single crack extends from the initial notch and its direction remains fixed throughout the fracture process. The transformation zone advances with the crack such that the leading edge of the zone moves with the crack tip during both stable and unstable crack growth. However, the trailing edge moves very little during stable crack growth resulting in an increase in the transformation zone size. During unstable crack growth the trailing boundary of the zone moves in a manner that keeps the zone size approximately constant. In all Group 1 specimens, the final fracture direction (measured in the plane of the specimen) is at 77° from the primary AM microstructure.

For orientations in Group 2, the fracture process is more complicated. Group 2 orientations have two microstructures that appear in significant amounts. They form in a diffuse region ahead of the notch. This is distinctly different from the well-defined transformation zone observed in Group 1 specimens. Cracks initiate as wing cracks and a single main crack grows from one of the wing cracks. The main crack does not appear to carry microstructure with it, as in Group 1. Also, there does not appear to be any correlation between the direction of the main crack and the direction(s) of the initial wing cracks. Except for orientation I, the main crack is straight and has an in-plane angle between 76° and 85° from the in-plane angle of the primary AM microstructure.

The differences in fracture behavior between the two groups reflect their different crystallography. Recall that Group 1 orientations (II, III and IV) have their initial notch near the [0 0 1] cubic direction, while Group 2 orientations have their initial notch close to the [1 1 0] cubic direction. An immediate consequence of this is that the ratio of the elastic modulus in the x_n-direction to that in the y_n-direction ($E_{11}/E_{22} = S_{22}/S_{11}$, see Vasko et al. (2002) for values) is dramatically different between Group 1 and

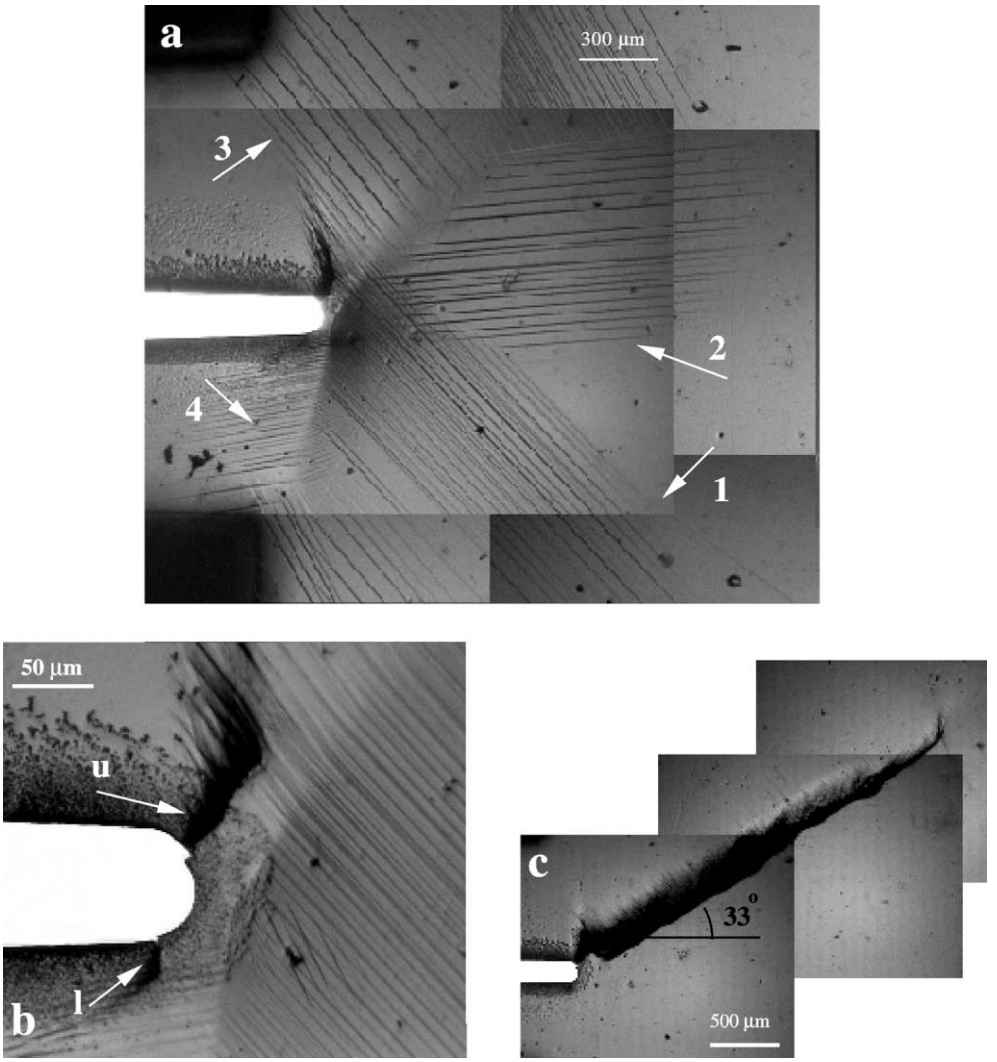

Fig. 16. A global view of the microstructure in specimen CT6 with orientation VII is shown in (a). Notch tip microstructures with in-plane angles of −47° (arrows '1' and '3') and 4.5° (arrows '2' and '4') are seen. The images (a) and (b) show stable growth of two wing cracks, marked by arrows in (b). Growth of the wing cracks is followed by unstable crack growth and failure. The view of the final crack after unloading is shown in (c). These images were taken at the following points on the load–displacement curve Fig. 17 at: (a) 5, (b) 6 and (c) 7.

Group 2 orientations. Specifically, because the [1 1 0] direction is stiffer than the [0 0 1] direction in CuAlNi, E_{11}/E_{22} for Group 1 orientations is less than one, while E_{11}/E_{22} for Group 2 orientations ranges from 2.82 to 3.15. This results in different stress fields in the two groups. For example, the microstructures predicted for Group 1 have the largest (or second largest) available work using either the plane stress or plane strain crack tip stress fields (see Vasko et al. (2002)), while the microstructures predicted for Group 2 have the largest available work only in the plane stress case; the plane strain calculation gives a completely different set of interfaces. The different stress fields can also affect crack kinking, as discussed below.

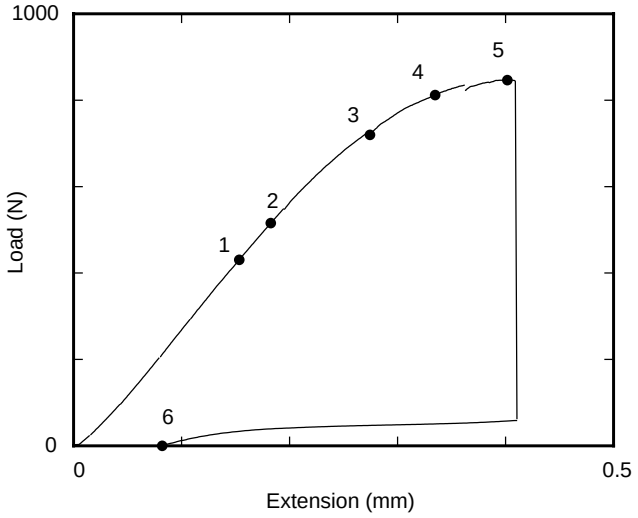

Fig. 17. The load–displacement curve for specimen CT6 with orientation VII is shown. The circles represent the load level associated with the images presented in this work.

There are two additional crystallographic differences between Groups 1 and 2, though their precise relationship with notch orientation and their effect on fracture behavior is unclear. First, the stress-induced microstructures in Groups 1 and 2 belong to different symmetry sets. Group 1 microstructures belong to the family described by the AM interface vectors $\mathbf{m} \in \langle 0.1430, 0.6679, 0.7304\rangle$ and $\mathbf{b} \in \langle 0.0237, 0.0559, 0.0707\rangle$, while Group 2 microstructures belong to the family described by $\mathbf{m} \in \langle 0.2607, 0.6345, 0.7276\rangle$ and $\mathbf{b} \in \langle 0.0122, 0.0653, 0.0654\rangle$. Second, the fracture planes are different between the two groups. Fracture planes were indexed macroscopically (Vasko, 2001) for the CT specimens with orientations II, III, IV, V, VII, and VIII [4] and their orientations are given in Table 3. The fracture planes for Group 1 are of type $\{765\}$, while those for Group 2 are close to $\{566\}$. It should be noted that neither of these corresponds to the likely $\{100\}$-type cleavage planes in CuAlNi (Zhdanov, 1965).

Table 3 shows that the in-plane angle between the fracture direction and the primary microstructure is consistently near 80° for all specimen orientations. This angle cannot be explained by crack direction criteria for a material with a homogeneous crystal structure (i.e., a non-transforming material). Specifically, it has been shown that crack kinking in the absence of transformation is predicted only for values of E_{11}/E_{22} greater than 4.0 (Azhdari and Nemat-Nasser, 1996), which is larger than this ratio for any of the orientations considered here. [5] However, it seems reasonable that the crack grows away from the transformed region. The transformation to martensite extracts energy from the crack tip elastic field, presumably near the martensite, and hence there is more elastic energy available for the fracture process in directions nearly perpendicular to the AM microstructure. However, it is difficult to quantify this idea because the AM microstructures are predicted based on constrained theory, that is, the AM interfaces are perfectly compatible with no local elastic relaxation (there is overall elastic relaxation due to the interaction with the loading device).

These rough energy arguments can also be applied to the fracture process. It is observed that the duration of stable crack extension depends strongly on the amount of the AM microstructure that forms before and

[4] Orientations I and VI were not considered.

[5] On the other hand, one may speculate that the fact that Group 2 orientations have significantly larger E_{11}/E_{22} ratios than Group 1 orientations may explain some features of the Group 2 behavior, for example wing cracking.

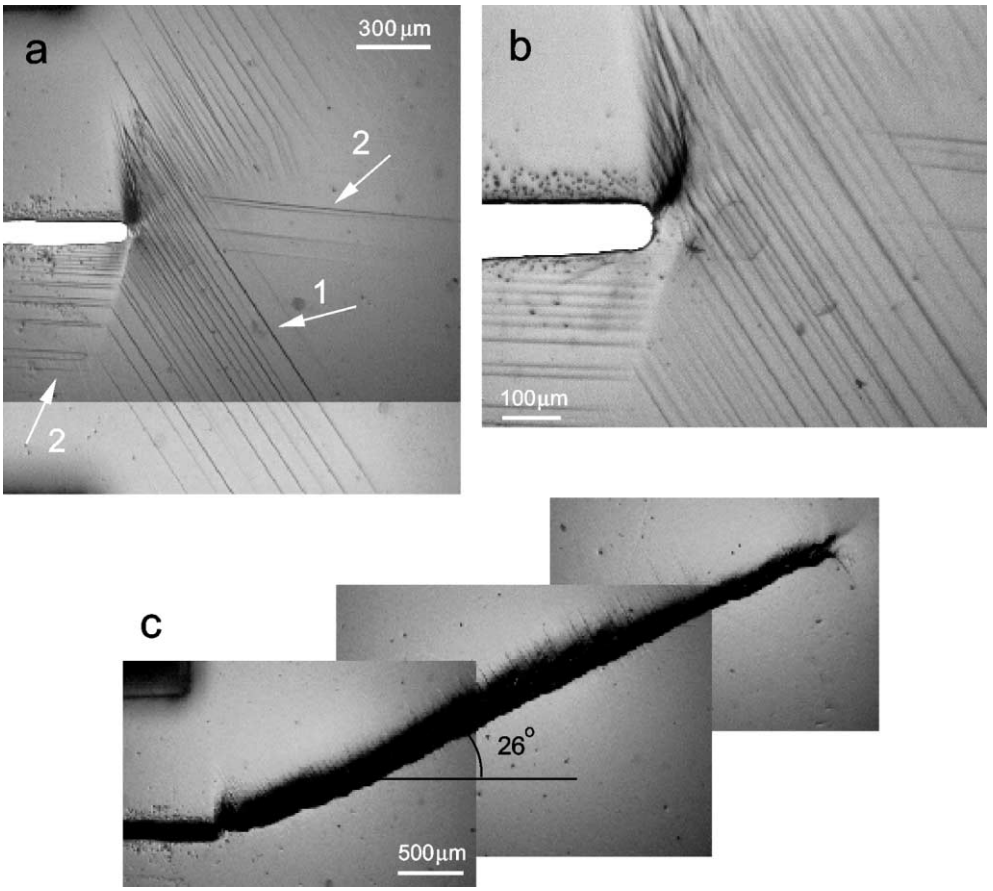

Fig. 18. The fracture process in specimen CT7 with orientation VIII is shown. Image (a) shows a global view of the specimen shortly after the wing crack initiates. The formation of microstructures with in-plane angles of −57° (arrow '1') and −3° (arrow '2') is seen. A higher magnification view of the wing crack is shown in (b). A view of the final crack after unloading is shown in (c). These images were taken at the following points on the load–displacement curve Fig. 19 at: (a) 5, (b) 4 and (c) 6.

during the fracture process. This is especially apparent in Group 1 orientations, which show a distinct transformation zone. Stable crack extension is accompanied by the formation of new microstructure at the crack tip. Detailed measurement verifies that this is an enlargement of the transformation zone and not a translation of it. This suggests that the energy required to form the transformation zone acts to stabilize the growing crack by reducing the energy available to form fracture surface. In this regard, it should be noted that stable crack propagation is accompanied by a *plateau* region of the load–displacement curve, which indicates that work by the loading device is split between the crack extension and formation of new microstructures, and does not increase the elastic energy of the system. In contrast, during unstable crack extension, a reverse transformation of the material to austenite occurs at the trailing edge of the zone, so the transformation zone translates rather than extends. While translation of the transformation zone will, in most cases, absorb energy (because of the hysteresis associated with the transformation), it is expected that the energy to translate the zone will be substantially less than that required to grow the transformation zone.

The effect of transformation on fracture process is also apparent when comparing the experimental results from SEN and MSEN specimens with orientation III. The primary microstructure (at −77°) in SEN

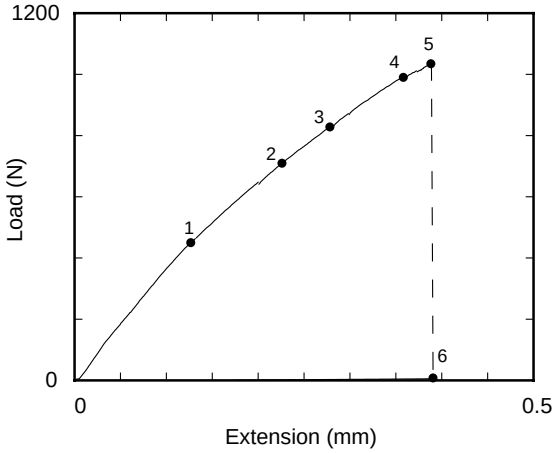

Fig. 19. The load–displacement curve for specimen CT7 with orientation VIII is shown. The circles represent the load level associated with the images presented in this work.

Table 3
A summary of fracture behavior for all orientations

Group	Orientation	Fracture direction		Angle between crack and microstructure	Fracture plane
		w.r.t. x_n	w.r.t. [0 0 1]		
1	II	22°	30°	77°	$(\overline{7}6\overline{5})$
	III	0°	30°	77°	$(\overline{7}6\overline{5})$
	IV	0°	−30°	−77°	$(\overline{7}65)$
2	I	0°/±32°	90°/±58°	±27°/±57°	n/a
	V	43°	−41°	76°	$(5\overline{6}6)$
	VI	−50°/ − 43°*	34°/41°*	−83°/ − 76°*	n/a
	VII	33°	−37°	80°	$(5\overline{6}6)$
	VIII	26°	−32°	85°	$(\overline{5}65)$

The angles marked with an asterisk were measured on the back of the specimen. The fracture direction is given relative to the x_n-direction and the [0 0 1] cubic axis in the $(1\bar{1}0)$ plane for all orientations. The fracture plane was determined by macroscopic optical measurements of the fracture surfaces.

specimen T7b (and T7a) with orientation III did not reach the free edge in the single edge notch specimen (see Fig. 8(b)). In this specimen no stable crack growth was observed. When the specimen shape was redesigned (MSEN specimen T9a) so that the −77° microstructure could reach a free edge, the amount of the transformed material dramatically increased compared to the SEN specimen and a stable crack growth regime was observed (Fig. 10(b)). This can be explained as follows. When a martensite plate ends inside the crystal, its tip is not compatible with undeformed austenite. Thus, the plate has an associated elastic energy, which increases with increasing plate thickness. As a consequence, there is no mechanism (other than fracture) to absorb loading energy without a load increase. Once the specimen was redesigned so that the martensite plate tip reaches the specimen edge, loading energy can be absorbed by additional transformation without a load increase, which in turn stabilizes the growing crack. This difference in fracture behavior is seen by comparing the load–displacement curves in Figs. 9 and 11. This behavior can be categorized as the effect of microstructural constraint, which can also occur due to grain boundaries, for example. It should be noted that all of the experiments reported here, except for the one just described, involve unconstrained microstructures.

6. Conclusions and future work

Experiments conducted over a range of initial notch orientations in single crystals of CuAlNi have shown that the fracture behavior of this material is strongly tied to the structural phase transformation it undergoes. The transformation significantly affects the fracture process and seems to control whether crack growth occurs in a stable manner or an unstable manner. The transformation acts as dissipative sink, competing with fracture, for the energy provided by the surroundings (the loading device). Because the amount of dissipation is limited by the amount of material that can be transformed in the neighborhood of the crack tip, the fracture eventually transitions from a stable regime to an unstable regime. The transformation also is tied to the fracture direction, such that the in-plane angle the AM microstructure makes with the fracture direction is in the range of 70–80° for all of the experiments.

Further work on this topic will study sets of orientations with notch tip directions along [1 0 0] and [1 1 1] in addition to the $[1\,\bar{1}\,0]$ direction considered here. A later paper will also develop the energetics of the transformation zone more fully. All of the experiments, with the exception of the SEN specimen for orientation T7b, were designed to give unconstrained microstructures. In most real systems, including polycrystals, such constraints will be present and their effect on the process of fracture in the presence of transformation requires further study.

Acknowledgements

TWS and GML would like to thank the Office of Naval Research under grant N00014-91-J-4034 for supporting this research. GML would also like to thank Zonta International for fellowship support during part of this research.

References

Azhdari, A., Nemat-Nasser, S., 1996. Hoop stress intensity factors and crack-kinking in anisotropic brittle solids. International Journal of Solids and Structures 33 (14), 2023–2037.

Birman, V., 1998. On mode I fracture of shape memory alloy plates. Smart Materials and Structures 7 (4), 433–437.

Dang, P., Grujicic, M., 1997. The effect of crack–tip material evolution in fracture toughness—an atomistic simulation study of the Ti–V alloy system. Acta Materialia 45 (1), 75–87.

Fang, D.-N., Lu, W., Hwang, K.C., 1999. Pseudoelastic behavior of CuAlNi single crystal under uniaxial loading. Metallurgical and Materials Transactions A—Physical Metallurgy and Materials Science 30A, 1933–1943.

Kim, J.W., Lee, E.S., Kim, T.J., Kim, Y.G., 1990. Microstructure and properties of grain-refined Cu–Zn–Al–X shape memory alloys. Journal of Material Science Letters 9 (4), 463–465.

Lai, M.O., Lu, L., Lee, W.H., 1996. Influence of heat treatment on properties of copper-based shape-memory alloy. Journal of Material Science 31 (6), 1537–1543.

Otsuka, K., Nakamura, T., Shimizu, K., 1974. Electron microscopy study of stress-induced acicular γ' martensite in Cu–Al–Ni alloy. Transactions of the Japan Institute of Metals 15, 200–210.

Rodriguez, C., Brown, L.C., 1976. Transition between stress-induced martensites in CuAlNi alloys. Metallurgical Transactions A 7A, 265–272.

Shek, C.H., Lin, G.M., Lai, J.K.L., Tang, Z.F., 1997. Fractal Fracture and Transformation Toughening in CuAlNi single crystal. Metallurgical and Material Transactions A 28A, 1337–1340.

Shield, T.W., 1995. Orientation dependence of the pseudoelastic behavior of single crystals of Cu–Al–Ni in tension. Journal of the Mechanics and Physics of Solids 43 (6), 869–895.

Shimamoto, A., Furuya, Y., Taya, M., 1996. Active control of crack–tip stress intensity by contraction of shape memory TiNi fibers. Intelligent Materials and Robots, 7th International Symposium, pp. 463–466.

Sih, G.C., Paris, P.C., Irwin, G.R., 1965. On cracks in rectilinearly anisotropic bodies. International Journal of Fracture Mechanics 1, 189–203.

Simha, N., Truskinovsky, L., 1994. Shear induced transformation toughening in ceramics. Acta Metallurgica et Materialia 42 (11), 3827–3836.

Sittner, P., Novak, V., Zarubova, N., 1998. Deformation by moving interfaces from single crystal experiments to the modeling of industrial SMA. International Journal of Mechanical Sciences 40 (2–3), 159–172.

Vasko, G.M., 2001. Ph.D. Thesis, University of Minnesota.

Vasko, G.M., Leo, P.H., Shield, T.W., 2002. Prediction and Observation of Crack Tip Microstructure in Shape Memory CuAlNi Single Crystals. Journal of the Mechanics and Physics of Solids 50, 1843–1867.

Wang, H., Wu, W., Wang, F., Yang, D., 1991. Dry sliding wear of Cu-based shape memory alloy. Acta Metallurgica Sinica 27 (6), 444–449.

Zhdanov, G.S., 1965. Crystal Physics. Academic press, New York and London.